Quaternary Science Reviews 169 (2017) 330–343

Contents lists available at ScienceDirect

Quaternary Science Reviews

journal homepage: www.elsevier.com/locate/quascirev

Younger-Dryas cooling and sea-ice feedbacks were prominent features of the Pleistocene-Holocene transition in Arctic Alaska

Benjamin V. Gaglioti [a, *], Daniel H. Mann [b], Matthew J. Wooller [c], Benjamin M. Jones [d], Gregory C. Wiles [e], Pamela Groves [f], Michael L. Kunz [g], Carson A. Baughman [d], Richard E. Reanier [h]

[a] Lamont-Doherty Earth Observatory of Columbia University, 61 Route 9w, Palisades, NY 10964, USA
[b] Department of Geosciences, University of Alaska Fairbanks, 900 Yukon Dr., Fairbanks, AK 99775, USA
[c] Water and Environmental Research Center, College of Fisheries and Ocean Sciences, University of Alaska Fairbanks, 306 Tanana Dr., Fairbanks, AK 99775, USA
[d] Alaska Science Center, US Geological Survey, 4210 University Dr., Anchorage, AK 99508, USA
[e] Department of Geology, The College of Wooster, 1189 Beall Ave., Wooster, OH 44691, USA
[f] Institute of Arctic Biology, University of Alaska Fairbanks, 902 North Koyukuk Dr., Fairbanks, AK 99775, USA
[g] School of Natural Resources and Extension, University of Alaska Fairbanks, P.O. Box 757140, Fairbanks, AK 99775, USA
[h] Reanier & Associates Inc., 1215 SW 170th St., Seattle, WA 98166, USA

ARTICLE INFO

Article history:
Received 27 February 2017
Received in revised form
4 May 2017
Accepted 12 May 2017
Available online 20 June 2017

Keywords:
Arctic Alaska
Paleoclimate
Oxygen isotopes
Climate change
Sea ice
Dendrochronology
Younger Dryas
North Pacific
Bering Strait

ABSTRACT

Declining sea-ice extent is currently amplifying climate warming in the Arctic. Instrumental records at high latitudes are too short-term to provide sufficient historical context for these trends, so paleoclimate archives are needed to better understand the functioning of the sea ice-albedo feedback. Here we use the oxygen isotope values of wood cellulose in living and sub-fossil willow shrubs ($\delta^{18}O_{wc}$) (*Salix* spp.) that have been radiocarbon-dated (^{14}C) to produce a multi-millennial record of climatic change on Alaska's North Slope during the Pleistocene-Holocene transition (13,500–7500 calibrated ^{14}C years before present; 13.5–7.5 ka). We first analyzed the spatial and temporal patterns of $\delta^{18}O_{wc}$ in living willows growing at upland sites and found that over the last 30 years $\delta^{18}O_{wc}$ values in individual growth rings correlate with local summer temperature and inter-annual variations in summer sea-ice extent. Deglacial $\delta^{18}O_{wc}$ values from 145 samples of subfossil willows clearly record the Allerød warm period (~13.2 ka), the Younger Dryas cold period (12.9–11.7 ka), and the Holocene Thermal Maximum (11.7–9.0 ka). The magnitudes of isotopic changes over these rapid climate oscillations were ~4.5‰, which is about 60% of the differences in $\delta^{18}O_{wc}$ between those willows growing during the last glacial period and today. Modeling of isotope-precipitation relationships based on Rayleigh distillation processes suggests that during the Younger Dryas these large shifts in $\delta^{18}O_{wc}$ values were caused by interactions between local temperature and changes in evaporative moisture sources, the latter controlled by sea ice extent in the Arctic Ocean and Bering Sea. Based on these results and on the effects that sea-ice have on climate today, we infer that ocean-derived feedbacks amplified temperature changes and enhanced precipitation in coastal regions of Arctic Alaska during warm times in the past. Today, isotope values in willows on the North Slope of Alaska are similar to those growing during the warmest times of the Pleistocene-Holocene transition, which were times of widespread permafrost thaw and striking ecological changes.

1. Introduction

Rapid climate changes often involve strong positive feedbacks, and in the Arctic the most important of these is the albedo change caused by reductions in the extent of sea ice in summer and early autumn (Serreze and Francis, 2006). Over the last 40 years, coverage of multi-year sea ice in the Arctic Ocean has decreased by 11% per decade (Screen and Simmonds, 2010), which is an alarming trend because general circulation models suggest a seasonally ice-free Arctic Ocean will have strong effects on global climate (Deser

* Corresponding author.
E-mail address: bengaglioti@gmail.com (B.V. Gaglioti).

http://dx.doi.org/10.1016/j.quascirev.2017.05.012
0277-3791/

et al., 2010). Recent observations of unusual convective storms traversing the Arctic Ocean and intense winters in mid-latitudes tend to support this prediction (Vihma, 2014; Klein et al., 2015a). Recent declines in sea ice have been forced by and acted to enhance warming air temperature trends in Arctic Alaska, including a 2.9 °C rise in mean annual temperature at Barrow (Fig. 1) since CE 1900 (Wendler et al., 2010), and a 0.5–2 °C rise in mean annual permafrost temperature over the last several decades (Smith et al., 2010; Jeffries et al., 2012). Sea-ice-enhanced warming of air temperatures could thaw permafrost and release its vast stores of ancient carbon downstream and to the atmosphere, which in turn could change global carbon budgets and influence climate and ecosystems across a wide range of spatial and temporal scales (Jorgenson et al., 2006; Schuur et al., 2008; Post et al., 2009; Bhatt et al., 2014).

A deeper historical context is needed to understand the potential magnitude, sensitivity, geographic extent, and ecological ramifications of the ice-albedo feedback. Land-based paleoclimatic records that are sensitive to both abrupt climate change and sea-ice-processes can provide this additional perspective with precisely dated paleo-records whose chronologies are not complicated by the ^{14}C-reservoir effects in marine records. The prehistoric precedents most comparable in their rates and magnitudes to the changes in sea-ice cover and climate occurring today occurred 17,000 to 8000 calendar ^{14}C years ago (17.0–8.0 ka) during the last deglaciation (Ruddiman, 2001).

The most notable of the warming events occurring during the last deglaciation was the termination of the Younger Dryas cold period at 11.7 ka when temperatures in Greenland warmed by at least 5 °C within a few decades (Alley, 2000). A sea-ice albedo feedback caused by the retreat of sea ice in the North Atlantic is thought to have amplified this post-Younger Dryas warming. The isotopic signature of this sea-ice retreat is recorded as a shift to both higher δ^{18}O values and deuterium excess values in Greenland ice cores as the evaporative source areas of Greenland-bound moisture moved northward over the Atlantic Ocean (Jouzel et al., 2005; Klein et al., 2015a).

Resolving the deglacial climate history in the Alaska–Siberia sector of the Arctic and how it compared with the North Atlantic region is critical for understanding the teleconnections and feedbacks of paleoclimatic events at high latitudes (i.e. Kaufman et al., 2004; Melles et al., 2012; Praetorius and Mix, 2014; Kaufman et al., 2016). Compared to the North Atlantic, much less is known about the postglacial climate history of the region surrounding the North Pacific, and the climate history of the Arctic Ocean and its adjacent lands remains a large gap in our understanding of paleoclimatic events (Polyak et al., 2010; Jakobsson et al., 2014).

In this study, we fill some of these knowledge gaps by building on the pioneering work of Epstein (1995) by using δ^{18}O values in modern and sub-fossil willow shrub (*Salix* spp.) cellulose ($\delta^{18}O_{wc}$) as a proxy for past climate change. Our focus is on the last deglaciation, 13.5 to 7.5 ka. We start by testing how climate variables affect the spatial and temporal patterns of $\delta^{18}O_{wc}$ values in living willows, and then, after compiling a record of ancient $\delta^{18}O_{wc}$ values, we infer how these climate variables changed during the Pleistocene–Holocene transition. Finally, we use this record to explore how abrupt deglacial climate changes both drove and were driven by Arctic sea-ice feedbacks.

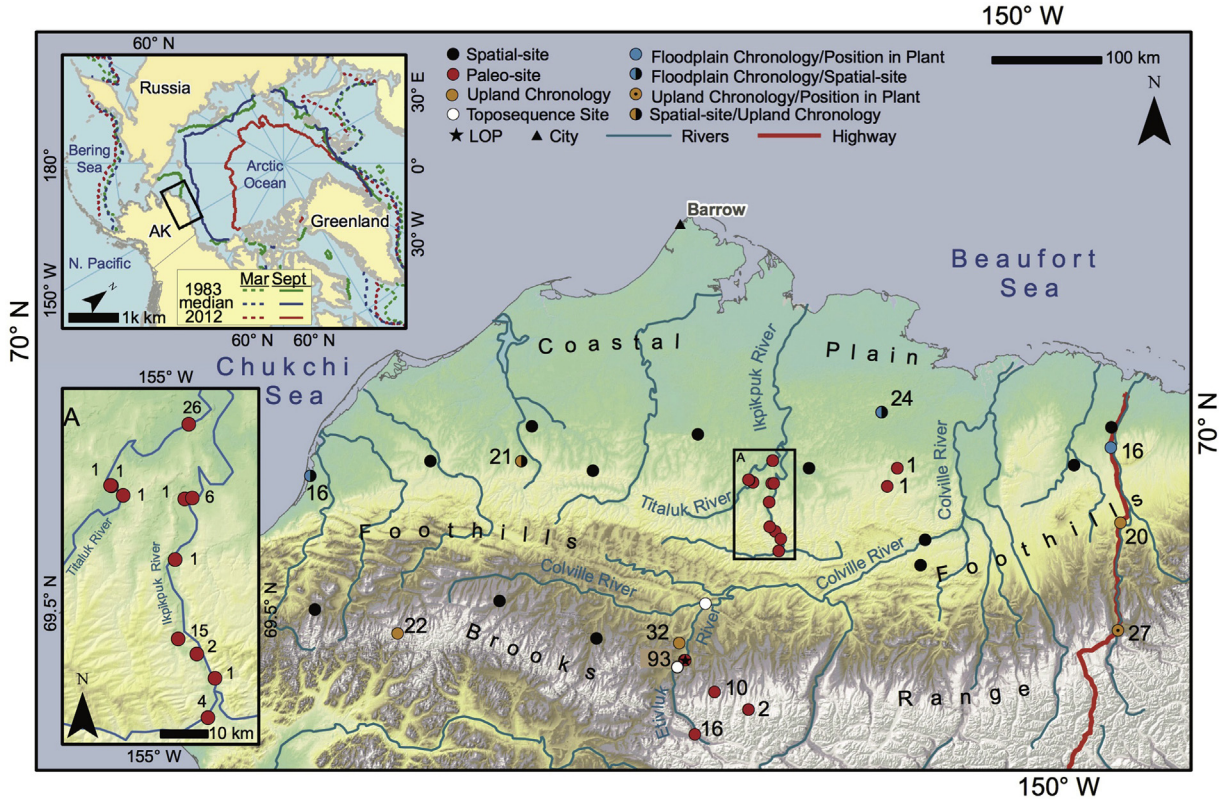

Fig. 1. Alaska's North Slope showing sampling locations. See text for site descriptions. Numbers next to 'paleo' and 'chronology' sites indicate how many sub-fossil (total = 179), and individual rings (total = 178) were analyzed for $\delta^{18}O_{wc}$ from these locations. Top left inset shows maximum (March; dashed line) and minimum (September; solid line) sea-ice extent during 1983 (green lines) and 2012 (red lines), which represent the most and least extensive sea-ice years since record keeping began in 1976. Also shown is the median sea ice extent since 1976 (blue lines; from Fetterer et al., 2002).

2. Regional setting

The study area is the North Slope of Alaska (Fig. 1), a region slightly larger than Great Britain that lies between the east-west trending Brooks Range and the Beaufort and Chukchi Seas of the Arctic Ocean. Today sea-ice covers much of the adjacent seas around the North Slope between December and July, reaching its maximum in March (Wendler et al., 2010). Sea-ice extent is minimum in September, and, in recent years, several thousand square kilometers of ocean has been open in the southern Beaufort and Chukchi Seas during late summer and early fall (Fetterer et al., 2002; Wendler et al., 2010). Sea ice extent tends to amplify seasonal and inter-annual temperature changes over the North Slope due mainly to ice albedo feedbacks (Wendler et al., 2010; Alexeev et al., 2016).

The North Slope lies above the Arctic Circle, is covered by tundra vegetation (Fig. 2) (Walker et al., 2005), and underlain by continuous permafrost (Jorgenson et al., 2008). A ~20- to 50-cm-thick active layer thaws each summer and refreezes every winter (Romanovsky and Osterkamp, 1995). The presence of both sea ice and the maritime effects of the Arctic Ocean to the north and west creates steep biophysical gradients in the region today, with both precipitation and growing season temperature declining towards the coast (Zhang et al., 1996). This results in lower primary productivity, less woody vegetation, colder soils, and thinner active layers as the coast is approached (Hinkel and Nelson, 2003; Walker et al., 2005).

Despite its cold climate, much of the North Slope was never glaciated during the ice ages because of its aridity (Ager et al., 2004). Today the North Slope has a semi-arid climate, and most precipitation originates from evaporative sources in the North Pacific Ocean and Bering Sea (Zhang et al., 1996). Air masses arriving from these distant seas are generally moisture-poor because they have rained-out while crossing wide continental expanses and mountain ranges (Moritz, 1979). During the few months in the late summer and autumn when sea-ice cover is at a minimum, precipitation on the North Slope is supplemented by moisture evaporating from the northern Bering, Chukchi, and Beaufort Seas (Homan, 2015). Recent reductions in sea-ice extent have been linked to increased precipitation in the Arctic (Kopec et al., 2016), with the effects most pronounced in summer and autumn when sea surface temperatures are warmest (Boisvert and Stroeve, 2015).

Due to the cold, waterlogged soil conditions and underlying permafrost, plant material, including pieces of subfossil wood, are well-preserved in a variety of depositional environments on the North Slope (Fig. 3) (Mann et al., 2002, 2010; Gaglioti et al., 2014; Baughman et al., 2015). A particularly long sedimentary archive containing abundant ancient wood material is provided by the partially drained basin of the informally named "Lake of the Pleistocene" (LOP) (Mann et al., 2002; Gaglioti et al., 2014). The LOP is located in the Arctic Foothills near the northern front of the Brooks Range (Fig. 1). The former bed of LOP is now exposed as a bluff along the Etivluk River (Figs. 1 and 3) (Mann et al., 2002; Gaglioti et al., 2014). Most of the ^{14}C-dated pieces of willow wood used in this study come from the LOP site (n = 93 out of n = 179); another suite of dated willow wood come from stratigraphic sections of terrestrial and fluvial sediment (Mann et al., 2010) exposed in the drainages surrounding LOP (n = 28 out of 179), as well as the Ikpikpuk and Titaluk Rivers located 150 km north of LOP at the southern margin of the Arctic Coastal Plain (n = 52 out of 179) (Fig. 1, bottom inset).

3. Methods

3.1. Approach: $\delta^{18}O$ in wood cellulose

Well-preserved ancient wood often retains the isotopic signatures of its former source water (McCarroll and Loader, 2004), and so the oxygen isotope composition of wood cellulose can provide useful and temporally-precise paleoclimate records (Epstein et al., 1976; Gray and Thompson, 1977; Yapp and Epstein, 1982; Epstein, 1995; Richter et al., 2008). The $\delta^{18}O$ of precipitation and the degree of evapotranspiration controls the $\delta^{18}O$ signal in wood cellulose (McCarroll and Loader, 2004). In turn, the $\delta^{18}O$ of precipitation is controlled mainly by four factors: 1) the initial isotopic composition of the moisture being evaporated, which in most cases comes from an ocean; 2) evaporative conditions at the moisture source including sea surface temperature, relative humidity, and wind speed; 3) the degree of cooling or Rayleigh distillation the air mass experienced, which is controlled by atmospheric temperature during condensation; and 4) any re-evaporation that occurred after initial condensation (Kendall and McDonnell, 2012). Because of the geographic and intra-annual variability in water isotopes within a given region, the key relationships that need to be understood before the $\delta^{18}O$ values in wood cellulose can be interpreted in terms of paleoclimate are: 1) the season that the plant's source water precipitated, 2) the weather conditions controlling isotopes in precipitation values in the particular study region, and 3) whether

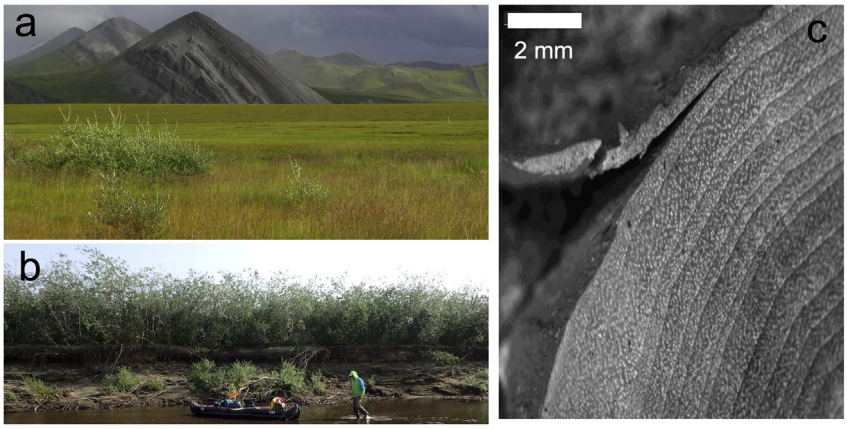

Fig. 2. a) A typical patch of upland willow shrubs in the foreground with the Arctic Foothills of the Brooks Range in the background. b) Floodplain willows (*Salix alaxensis*) along the Titaluk River behind the canoe for scale. c) Sanded cross section of a willow stem under a dissecting microscope. Outer ring is being removed with a scalpel for cellulose extraction and $\delta^{18}O$ analysis.

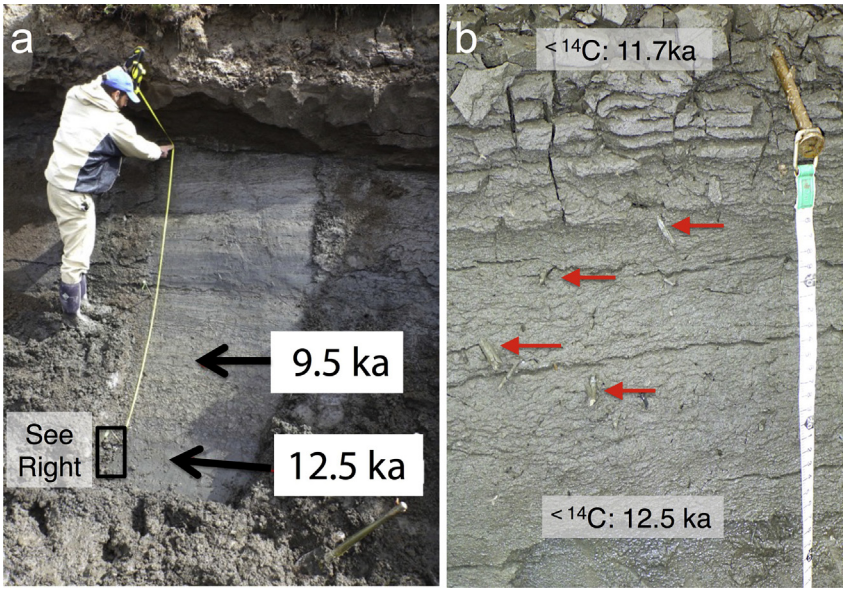

Fig. 3. a) Sampling Lake of the Pleistocene (LOP) section with locations of two ^{14}C dates indicated. b) Close-up of LOP exposure. Arrows point to fragments of ancient willows that were analyzed for $\delta^{18}O_{wc}$. Calendar-age estimates from individual willow twigs are based on either their ^{14}C ages or on interpolated ages. (Gaglioti et al., 2014). In right-side panel, measuring tape extends 32 cm.

the precipitation signal was significantly altered by evaporation and/or by transpiration (McCarroll and Loader, 2004). In order to know when isotopic change is related to climate rather than the internal variability of a stem or site, it is also important to document how $\delta^{18}O_{wc}$ values vary between growing sites and within different parts of the same plant (Leavitt, 2010). Once these climate-plant-cellulose isotope relationships are established in the present day and their variability is quantified, time series of ancient wood isotopes can then be used to infer past climate changes (Burk and Stuiver, 1981; Porter et al., 2009; Brienen et al., 2012).

Physiological fractionation processes also have the potential to modify the precipitation-related isotopic signatures registered in wood cellulose. These physiological processes include: 1) transpiration that can cause ^{18}O-enrichment, which is enhanced when plants experience drought stress (Roden et al., 2000; McCarroll and Loader, 2004), 2) oxygen-isotope fractionation of ~ +27‰ occurring when plant sucrose (a precursor of cellulose) is formed (Sternberg et al., 1986), and 3) the degree that transpiration-altered phloem water exchanges with unaltered xylem water coming up from the roots when they meet in the stem and fuel cellulose production (Roden et al., 2000). Comparing how $\delta^{18}O$ values relate to $\delta^{13}C$ values from the same cellulose samples can determine how much transpiration tends to modify these climate signals because higher $\delta^{13}C$ values indicate higher rates of water use efficiency, and lower rates of transpiration (Lambers et al., 1998). Although these physiological processes can modify cellulose $\delta^{18}O$ values, in general they are often subordinate to broad geographic patterns and long-term climate change (millennia) in $\delta^{18}O_{wc}$ determined by meteorological and oceanographic factors affecting initial evaporation, transport, and condensation of precipitation (Gray and Thompson, 1977; Yapp and Epstein, 1982; Epstein, 1995; Porter et al., 2009; Brienen et al., 2012).

3.2. Sampling

We sampled modern willows in order to understand what climatic, site-specific, and within-plant processes have influenced $\delta^{18}O_{wc}$ values on the North Slope of Alaska over the last few decades (Supplemental Table 1). Willows (genus *Salix*) are the most common shrubs in low arctic tundra vegetation where upright woody plants exist near the northern limit of their range. The modern willows we sampled were 0.5- to 3-m-tall shrubs growing in a variety of topographic settings (Fig. 2; Supplemental Table 1). We compared the $\delta^{18}O_{wc}$ values of individual annual rings (Fig. 2c) with monthly climate variables from the current and previous year of growth ('dendro samples', orange and blue dots in Fig. 1). For these dendro samples, living willows were sampled by cutting basal cross-sections from five individuals growing at eight, widely separated upland or floodplain sites consisting of *Salix alaxensis* (Andersson) Coville and *Salix glauca* L. (Fig. 1). Cross-sections were incrementally sanded with up to 600-grit sand paper. Using a Velmex measuring machine, we manually measured ring widths on at least two radii from each of the five individuals from each location, and then cross-dated the ring series within and between the samples, checking the dating using the COFECHA program (Supplemental Table 1; Holmes, 1983). Individual rings from eight cross-dated individuals (one from each location) representing various time windows from CE 1976 to 2012 ($n = 178$ total ring years; Fig. 1; Supplemental Table 1) were sampled with a scalpel under a dissecting microscope (Fig. 2c).

We then compared the average $\delta^{18}O_{wc}$ values of homogenized, whole stems from multiple willows growing at different sites with mean climate variables for that location (mean of CE 1976 to 2012; 'spatial samples', black dots in Fig. 1) to determine how $\delta^{18}O_{wc}$ varied across the region. Wood from spatial samples was collected in the same manner as described above from 15 different locations, but cross-sections were not measured for ring-widths or cross-dated. Each stem was homogenized so that each sample represented the entire cross-section of one individual shrub, with the five samples from each site representing five different individuals. Spatial samples consisted of a variety of upright species (hereafter all modern and paleo-*Salix* spp. are termed 'willow'). For spatial samples, an average of all $\delta^{18}O_{wc}$ values was then taken for each location and used for kriging analysis to make an interpolated map of $\delta^{18}O_{wc}$ values of the western North Slope as described below.

To estimate the intra-site variability in $\delta^{18}O_{wc}$ values, we used

individual growth rings representing the same year from five different individuals growing at the same site (white, 'toposequence' dot near the Colville River and the LOP site in Fig. 1). We also looked at the variability of individual $\delta^{18}O_{wc}$ values among individual willows and individual rings at the same site at each of the twenty study locations (shown in Fig. 1). Because ancient samples were likely composed of wood from various heights on a stem, we also wanted to know how $\delta^{18}O_{wc}$ varies within an individual shrub ('position in plant' sites in Fig. 1). To do this, we sampled and analyzed the same annual ring at three to four different heights in the stem of a modern willow between its root crown and terminal twig.

To extend our record back in time, we analyzed ancient wood from geologic sections (Mann et al., 2002, 2010; Gaglioti et al., 2014; Baughman et al., 2015) that was identified as either willow (n = 167) or cottonwood (*Populus balsamifera* L.; n = 12) (Figs. 1 and 3). All wood fragments from the LOP section are assumed to be willow because it is the most common shrub surrounding the lake today, and – based on the pollen record from this lake (Mann et al., 2002) – it has been common there over the past 14.5 ka. In addition, we identified hundreds of willow leaves from the LOP section, and found no shrub birch (*Betula* spp.) or alder (*Alnus* spp.) leaves, the other upright shrub taxa growing in the region today. Wood that was sampled from other stratigraphic sections was identified as willow if it did not have cottonwood or conifer bark characteristics. Cottonwood has a characteristic thick, furrowed bark with a thin, persistent inner bark. Most of the cottonwood we encountered were large-diameter (>15 cm) tree trunks.

In total, we analyzed 179 samples of ancient wood ranging in size from logs to twigs and ranging in age from ~0.3 ka to >45.0 ka. Some wood samples were directly radiocarbon dated by the AMS technique (n = 70, Supplemental Table 2). The remainder came from stratigraphic sections possessing secure age-depth relationships that could be used to interpolate the ages of individual samples. The modeling techniques used to generate these chronologies are described in Gaglioti et al. (2014) for LOP and in Baughman et al. (2015) for the Lawrence's Bend meander scroll site (Fig. 1).

3.3. Cellulose extraction and isotope analysis

Alpha-cellulose (α-cellulose) is the preferred compound from which to infer source-water isotopes (Gray and Thompson, 1977; Schleser et al., 1999; Roden et al., 2000; McCarroll and Loader, 2004; Szymczak et al., 2011). We used the Jayme and Wise method to extract holocellulose from batches of 50–75 crushed wood samples (Green, 1963). Instead of using glass filter paper to extract samples (as in Leavitt and Danzer, 1993), we used synthetic polymer fiber pouches (F57 filter bags from the Ankon Technology Corporation). Alpha-cellulose extraction then followed the methods of Green (1963), but instead of the ethanol and benzene baths we used ethanol and toluene baths in a soxhelet apparatus to reduce carcinogen exposure as is recommended by Leavitt and Danzer (1993). Samples were then rinsed in deionized water (DI), boiled in DI, and then stirred in a solution of 0.006 L glacial acetic acid: 1.8 L DI and 12 g of sodium chlorite for 1 h at room temperature. Sample pouches were then stirred in a solution of 0.17 kg pelletized NaOH dissolved in 1 L DI for 1 h at room temperature. Ancient cellulose samples that showed signs of iron oxide deposits were boiled in 0.15 M solution of oxalic acid for 90 min. This was done because iron oxides from geologic sources can alter the $\delta^{18}O$ values of cellulose and therefore need to be removed (Leavitt and Danzer, 1993; Richter et al., 2008). Pure white α-cellulose samples with a mass of 0.3–0.5 mg were freeze-dried, weighed, and analyzed for stable oxygen isotope ratios on a Thermo Thermal Conversion Elemental Analyzer (TC/EA) attached via a Conflo III to a Thermo Delta V Plus isotope ratio mass spectrometer (IRMS) at the Cornell University Stable Isotope Laboratory. All $\delta^{18}O$ values are expressed relative to Vienna Standard Mean Ocean Water (VSMOW). The consistency of the cellulose extraction process was tested by comparing the $\delta^{18}O$ values from analyses of replicate samples composed of a homogenized ancient wood standard (Porter and Middlestead, 2012), where nine samples were extracted and analyzed in two different batches, and three standards were extracted and analyzed in a third batch. The ancient wood standard replicates had a $\delta^{18}O_{wc}$ standard deviation of 0.46‰ (n = 9), 0.23‰ (n = 9), and 0.34‰ (n = 2) respectively, for each of the tested batches and a total standard deviation of 0.95‰ (n = 21). Analytical precision was estimated by multiple analyses (~15 standards for every 50 samples) of the IAEA standards including 601, 602, Benzoic Acid, and C4. Replicates of these standards had a $\delta^{18}O$ standard deviation range of 0.29‰–0.87‰ within each of the batches. We only analyzed cellulose samples that had a 40–55% oxygen (O) content, which is near the ~50% O content of pure cellulose. Lower values in paleo-samples imply that some cellulose degradation had occurred, and the $\delta^{18}O_{wc}$ values might have experienced fractionation from diagenesis or other factors not related to source-water changes in the past. We also analyzed the cellulose extracted from spatial samples for $\delta^{13}C$ to determine whether there was any relationship between site-standardized $\delta^{18}O_{wc}$ and site-standardized $\delta^{13}C_{wc}$ (n = 15 sites, n = 5 individuals from each site), which would indicate that $\delta^{18}O_{wc}$ values are significantly altered by transpiration.

3.4. Data analysis

The $\delta^{18}O_{wc}$ values from each dendro location were standardized by site (annual isotope value – mean/standard deviation), and compared with interpolated mean monthly and annual temperatures and precipitation (1976–2012) from the Climate Research Unit's gridded temperature and precipitation (CRU TS3.22) dataset interpolated at 0.5° intervals (Harris et al., 2014). We also used mean values from each of the sample sites to interpolate the mean $\delta^{18}O_{wc}$ values using the kriging algorithm in ArcMap 10.3 to assess the potential coast-to-inland $\delta^{18}O_{wc}$ gradient recorded in willow shrubs and therefore in precipitation isotopes across the North Slope. We then compared individual ring site-standardized $\delta^{18}O_{wc}$ values with spatially interpolated, site-standardized mean monthly temperature and precipitation for both the current (growing season) year and for the preceding year using the CRU TS3.22 dataset as a time series (Harris et al., 2014). Site standardizing was done to remove the spatial effects of climate and $\delta^{18}O_{wc}$ values when combining sites. Site-standardized $\delta^{18}O_{wc}$ data from dendro samples were also compared with the monthly sea-ice extent for the previous year estimated for a geographic window encompassing 65°–75° N and 170° to 135°W, a region encompassing the northern Bering, Chukchi and Beaufort Seas from approximately the longitude of eastern Chukotka eastward to the Mackenzie River delta (Fig. 1; Fetterer et al., 2002). Pearson product-moment correlation coefficients (hereafter R) were calculated for each monthly and annual variable. Coefficients were deemed significant where p-values were <0.05.

The ages assigned to ancient $\delta^{18}O_{wc}$ values represent the median calibrated ^{14}C age of the wood sample or its mean interpolated age using age-depth modeling (reported in Gaglioti et al., 2014; Baughman et al., 2015). All ^{14}C ages were calibrated using the IntCal13 calibration curve (Reimer et al., 2013). For the period between 13.5 and 7.5 ka, $\delta^{18}O_{wc}$ values were smoothed using a locally weighted smoothing spline method (LOWESS) with a span of 0.3 (Cleveland and Devlin, 1988). Cross-validation using least squares

techniques were used to identify the LOWESS span length with the lowest root of the mean square error of prediction (in this case a 0.3 span) (Cleveland and Loader, 1996). The 95% confidence interval of this smoothed line was then used to compare whether different time periods had significantly different mean $\delta^{18}O_{wc}$ values.

The Rayleigh distillation model described by Kendall and McDonnell (2012) was used to explore the effects of different climatic and oceanographic scenarios on the $\delta^{18}O_{wc}$ patterns observed on the North Slope. We estimated $\delta^{18}O_{wc}$ values on the North Slope under different scenarios by calculating the estimated temperature difference between the oceanic evaporative sources (T_{source}) and the condensation site (T_c) and then compared these estimates with the observed changes in paleo-$\delta^{18}O_{wc}$ values and therefore in paleo-$\delta^{18}O_{precip}$ values. To correct for fractionation occurring during sucrose formation in plants, we converted $\delta^{18}O_{wc}$ values to $\delta^{18}O_{precip}$ values by subtracting 27‰ from $\delta^{18}O_{wc}$ (Sternberg et al., 1986). Equilibrium fractionation factors for evaporation and precipitation for different estimated ocean and air temperatures were calculated using Majoube (1970, 1971). Kinetic fractionation factors of evaporation under 10% humidity were calculated using those reported by Clark and Fritz (1997). The fraction of water lost during air mass cooling was calculated using water vapor saturation under different air temperatures (Goff and Gratch, 1946).

We adjusted the paleo $\delta^{18}O_{wc}$ values to remove the effects of a changing mean ocean isotope value due to sea-level drawdown during the last glaciation. For example, $\delta^{18}O_{wc}$ in willows estimated to be growing ~13.0 ka were taking up precipitation from an ocean that was 0.9‰ more enriched than the modern ocean value (VSMOW or 0‰). Therefore, to correct for these non-climatic source effects on precipitation, we subtracted the ocean values from the paleo-$\delta^{18}O_{wc}$ values so willows growing from the last 40 ka could be compared with each other and so that their temporal patterns would be unaffected by ocean source water isotopes. To continue with this example, the 13.0 ka $\delta^{18}O_{wc}$ values that were 17‰ were corrected to 16.1‰ so they could be compared with $\delta^{18}O_{wc}$ from other times including the modern willows. We used the 100-year estimates of mean ocean water $\delta^{18}O$ values based on Bintanja et al. (2005).

4. Results

4.1. Modern $\delta^{18}O_{wc}$ values and variability

We observed a disparity (mean difference of 4.5‰) between the whole-stem spatial samples and individual tree rings from the same stems. This difference is related to the presence of bark in the whole-stem samples, which in five pairs of samples we found is 4–8‰ lower than the wood of the same stem. Therefore, we corrected the whole-stem samples by adding to them the mean difference between all the whole wood *versus* stem samples (4.5‰). This bark offset is not relevant for comparisons between the dendro and paleo samples because all of those samples had their bark removed. Therefore, the bark effect is only relevant for comparing the modern dendro and modern spatial samples. This correction was further justified by the fact that the general spatial patterns of $\delta^{18}O_{wc}$ across the North Slope (see below) were similar for both the bark-on and bark-off samples, implying the bark fraction was the cause of this offset.

The mean $\delta^{18}O_{wc}$ value from individual rings (dendro samples; n = 178) growing between CE 1976 and 2012 was 18.03‰ (1.46‰ standard deviation). The intra-site variability of $\delta^{18}O_{wc}$ values for the samples representing the same year's growth ring in different individuals ranged from 0.64‰ (1 standard deviation, n = 6, CE 2011 ring, LOP site) to 0.76‰ (n = 8, CE 2012 ring, Colville River Site). Variability among homogenized individuals at the same site (spatial samples) ranged from 0.5‰ to 1.3‰ (1 standard deviation for n = 5 at each of 14 sites). Similarly, variability among different rings sampled from the same cross-section (i.e., dendro samples from same stem and radius) was 0.6‰–1.6‰ (1 standard deviation for each site). For intra-plant comparisons of $\delta^{18}O_{wc}$ values, outer ring values from cross-sections growing higher in the stem were generally lower by 1–2‰ (n = 3, for each of 3 individuals at one site; 1 standard deviation ranged from 0.41 to 1.2‰ for each individual). Because the intra-stem (1.5‰), intra-site (1.0‰), and inter-site (1.5‰) isotopic variability has been estimated from modern willow samples, we can calculate the magnitude of isotopic shifts in the paleo record that cannot be explained by this combined uncertainty. We estimate the additive uncertainty in paleo isotopic shifts by taking the sum of squares of the one-sigma uncertainties and adding the analytical uncertainty (0.87‰), which gives a combined uncertainty of 2.5‰. Overall, these data indicate that any shift in mean $\delta^{18}O_{wc}$ values > 2.5‰ likely represent significant shifts in the climatic factors controlling $\delta^{18}O_{wc}$ values.

Climate, geography, and annual variations in sea-ice extent were all found to significantly influence $\delta^{18}O_{wc}$ values in living willows (Figs. 4 and 5). For dendro samples from upland sites, average annual temperature during the growing season year, and particularly average June temperature were significantly, and positively correlated with $\delta^{18}O_{wc}$ values (Fig. 4; n = 115, R range = 0.31–0.32, p-value = 0.0007). In contrast, the $\delta^{18}O_{wc}$ values of floodplain willows were negatively correlated with average August temperature during the previous growing season (not shown; n = 63, R = −0.26, p = 0.04), but generally had low correlations for other months. For willows growing in both floodplain and upland settings, those individuals growing at the sites closer to the Chukchi and Beaufort Sea (Fig. 1) generally had higher $\delta^{18}O_{wc}$ values than those growing further away, which is also reflected in the modeled isotopes in precipitation of the region (Bowen and Wilkinson, 2002). Assuming that willows growing across this spatial gradient are consuming the same seasonal mix of precipitation and soil water, this pattern suggests that the Arctic Ocean is likely a significant moisture source for the precipitation used in recent willow growth (Fig. 5). This spatial pattern is unlikely to be related to changes in local air temperature because sites further away from the Arctic coast typically have warmer summer temperatures (Zhang et al., 1996), and therefore would be expected to yield the opposite trend in $\delta^{18}O_{wc}$ (higher $\delta^{18}O_{wc}$ values further inland). Site standardized $\delta^{13}C_{wc}$ values were not significantly correlated with $\delta^{18}O_{wc}$ values from the same samples (n = 80, R = 0.065, p-value = 0.57), indicating that climate-driven changes in water use efficiency or transpirational processes are not significant drivers in $\delta^{18}O_{wc}$ variability on the North Slope today.

Consistent with the coastal-enrichment result, the mean extent of sea ice surrounding the North Slope of Alaska during June, July, and August is negatively correlated with $\delta^{18}O_{wc}$ values in upland willows (Fig. 5; n = 115, R = -0.33, p-value = 0.0003). The residuals of a linear model between $\delta^{18}O_{wc}$ and mean June temperature (n = 115, R^2 = 0.09, p-value = 0.0006) were also negatively correlated with mean sea ice extent (not shown; n = 115, R = −0.26, p-value = 0.005). Thus, sea-ice extent seems to be a real driver of $\delta^{18}O_{wc}$ values, and more than simply an indirect, covariant effect between sea ice and summer temperature (n = 34, R = 0.81, p-value<0.0001). There are no significant correlations between the dendro $\delta^{18}O_{wc}$ values and precipitation amount. Taken together, these results indicate that, assuming climate–proxy stationarity, $\delta^{18}O_{wc}$ values from upland willows can be used to infer past climatic conditions (mean annual temperature, and specifically mean June temperature), as well as to infer changes in the oceanic source areas of precipitation that are influenced by temporal changes in regional sea-ice extent.

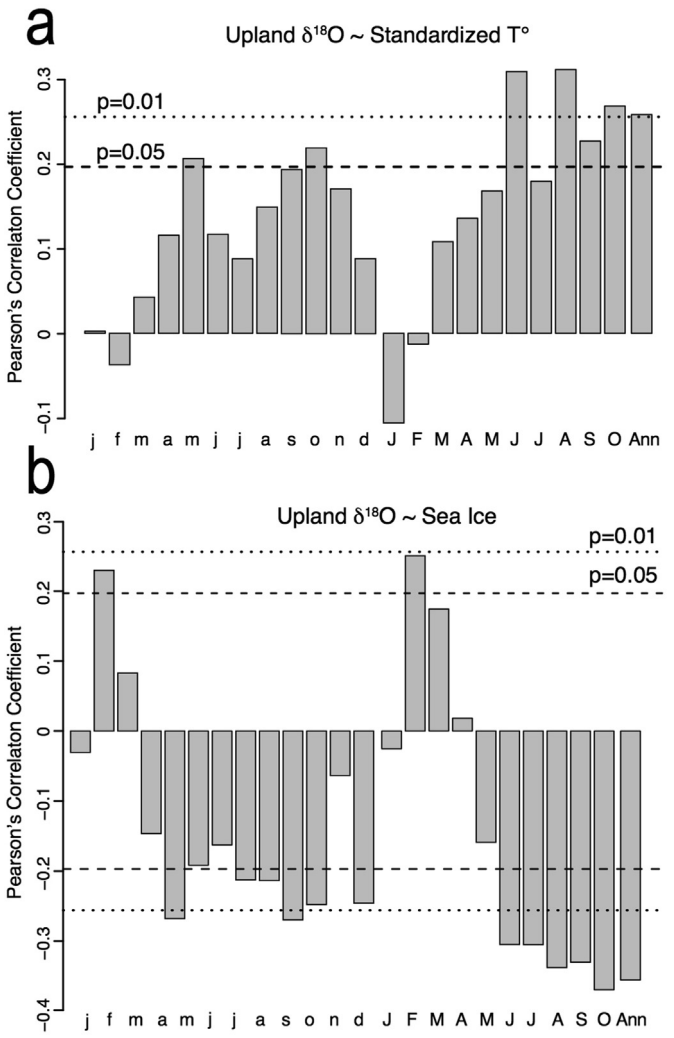

Fig. 4. Correlation coefficients between $\delta^{18}O_{wc}$ values of individual rings in cross-dated shrubs and monthly and annual climate variables in the previous year (lowercase letters) and growing season year (uppercase letters; annual growing season year is January–September) from upland willow sites (one shrub from eight sites combined to for 118 total ring years). a) Shows correlations between $\delta^{18}O_{wc}$ and air temperatures interpolated to 0.5°, and b) shows correlations between $\delta^{18}O_{wc\ and}$ sea ice extent surrounding the North Slope of Alaska (65°–75° N and 170°–135° W).

4.2. Paleo-$\delta^{18}O_{wc}$ values

The $\delta^{18}O_{wc}$ values of the 28 wood samples with ^{14}C ages >16.0 ka are on average lower than samples with ages <16.0 ka (Fig. 6). Significant fluctuations are apparent in both the raw and smoothed $\delta^{18}O_{wc}$ values that are younger than 13.5 ka (Fig. 7). $\delta^{18}O_{wc}$ values reached a peak ca. 13.2 ka, the highest smoothed value observed in the record, before declining by ~4.5‰ and reaching their lowest values ca. 12.1 ka. Between 12.0 and 11.0 ka, a ~4‰ increase in $\delta^{18}O_{wc}$ values occurred that peaked ca. 11.2 ka. A gradual decline of around 1.5‰ occurred between 11.2 and 10.0 ka. Six ancient samples dating to various times over the last 7 ka have a mean and standard deviation of 16.2‰ and 1.3‰, respectively, which overlaps with the $\delta^{18}O_{wc}$ values in wood dating to between 10 and 7.5 ka (Fig. 6). Living willows have elevated $\delta^{18}O_{wc}$ values compared with the early Holocene mean (Fig. 7). Individual, raw $\delta^{18}O_{wc}$ values similar to the mean of modern willows (18.03‰) last occurred ca. 13.2 ka and then sporadically between 11.3 and 9.0 ka (Fig. 7), however, modern willows have higher $\delta^{18}O_{wc}$ values than the mean smoothed paleo-samples from any point in the deglacial record (highest value is 16.3‰ at 13.2 ka).

5. Discussion

5.1. How $\delta^{18}O_{wc}$ values relate to past and present climate

The values of $\delta^{18}O_{wc}$ preserved in the wood cellulose of willow shrubs provide a proxy for climate history on the North Slope of Alaska and specifically for changes in air temperatures and precipitation sources. Here we focus on upland willows because they make up the vast majority of paleo-samples that we use to interpret these patterns (144 out of 179 total samples). Over recent decades, the temporal patterns of $\delta^{18}O_{wc}$ in upland willows correlate positively with mean annual and specifically June air temperatures (Fig. 4). Similar climate-isotope relationships are observed in high latitude conifers in the Northwest Territories of Canada and the Yakutia region of Siberia (Porter et al., 2009; Sidorova et al., 2010). Based on the effects that regional air temperature has on precipitation isotopes by Rayleigh distillation processes, warmer temperatures on the North Slope should reduce the rain-out of ^{18}O and cause higher $\delta^{18}O_{precip/wc}$ values both today and in the past (Kendall and McDonnell, 2012).

Sea-ice extent also influences $\delta^{18}O_{wc}$ values in North Slope willows, and we would expect changes in sea-ice coverage to accentuate temperature-driven $\delta^{18}O_{precip/wc}$ effects. This is because the extent of sea ice controls how much of the precipitation falling on the North Slope was evaporated from the nearby regions of the Arctic Ocean and Bering Sea. Under warmer conditions, retracted sea ice exposes more open water that serves as an evaporative moisture source, which supplies relatively elevated $\delta^{18}O_{precip}$ values to the North Slope willows compared with moisture coming exclusively from distant southern sources during colder periods when sea ice is more extensive. The effect of sea-ice extent on $\delta^{18}O_{wc}$ is illustrated by a steep gradient stretching inland from the Chukchi and Beaufort Sea coasts, indicating an Arctic source for the moisture fueling willow growth in recent decades (Fig. 5).

Other data sources corroborate the importance of the Arctic Ocean-derived moisture source we infer here based on the spatial patterns of $\delta^{18}O_{wc}$ in North Slope willows. Storm-track modeling coupled with isotopic measurements of precipitation events at Barrow, Alaska (Fig. 1) show that precipitation coming from evaporative sources in the ice-free Beaufort and Chukchi Seas has higher $\delta^{18}O$ values than distal sources (Bering Sea and Pacific Ocean) in part because these northerly air masses have undergone less cooling and rainout than southerly ones (Putman, 2013). As a result, Arctic Ocean-derived moisture leaves a distinct, positive $\delta^{18}O$ signal in ice from the McCall Glacier in northeast Alaska (Klein et al., 2015b). Hind casting of storm tracks has also shown that at times of the year when sea ice is far offshore, the Arctic Ocean has been the dominant moisture source for Alaska north of the Brooks Range (Putman, 2013; Homan, 2015).

Disentangling sea-ice versus temperature effects on $\delta^{18}O_{wc}$ in North Slope willows is complicated by the fact that inter-annual sea-ice extent correlates strongly and positively with inter-annual air temperatures over recent decades ($R = 0.81$). This is the case because sea-ice extent is partly controlled by summer air temperature, and because ice coverage then amplifies warming and cooling through albedo effects (Wendler et al., 2014; Alexeev et al., 2016). The very low $\delta^{18}O_{wc}$ values we find during the coldest periods of the last ice age (>16.0 ka; Fig. 6) occurred at times when perennial sea-ice covered the entire Arctic basin (Caissie et al., 2010; Polyak et al., 2010), and attest to the mutually reinforcing effects that low air temperatures and extensive sea-ice cover have on $\delta^{18}O_{wc}$. However, correlations between sea-ice extent and

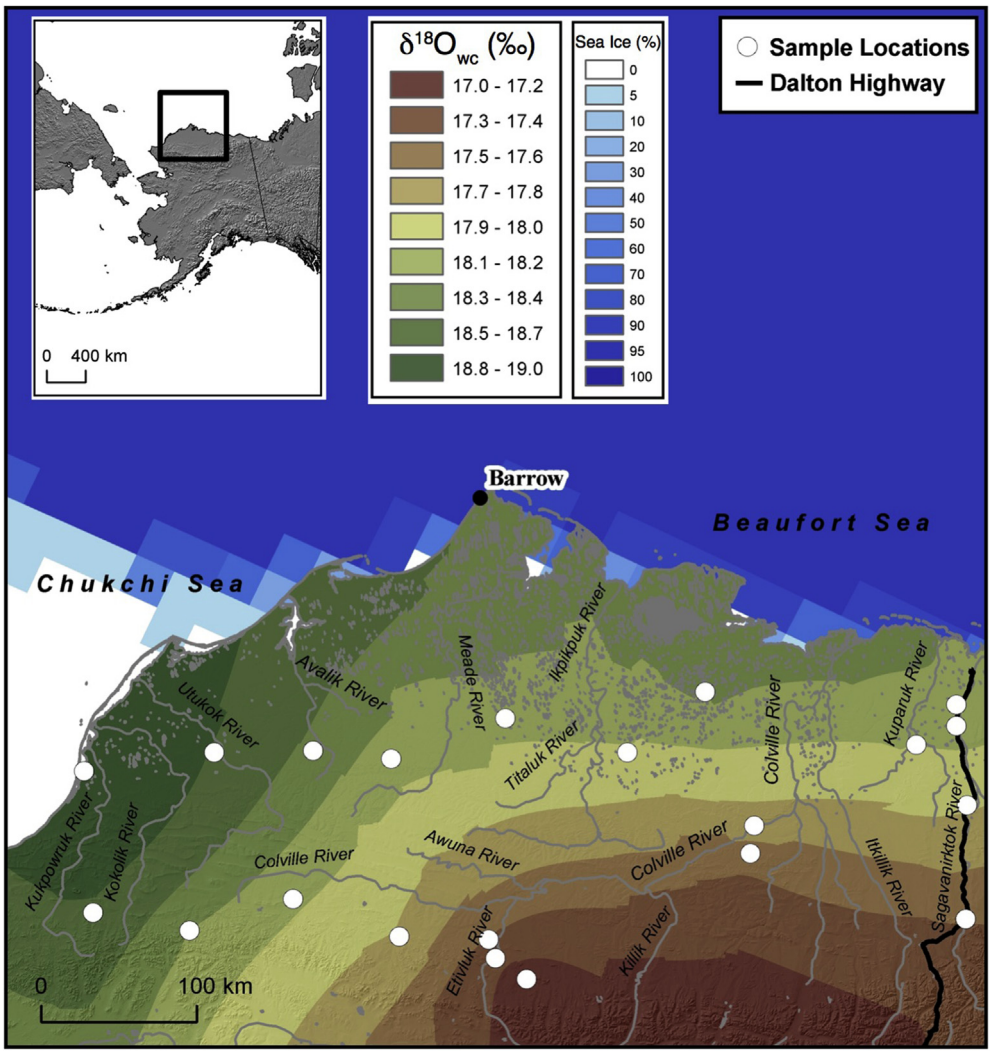

Fig. 5. Interpolated mean $\delta^{18}O_{wc}$ values for willow shrubs growing at 21 sites on the North Slope of Alaska. Sample means come from isotope analysis of whole stem and individual rings from willow shrubs. This represents a total of 263 samples from 88 individual shrubs. Shades of white to blue indicate the percent of July sea-ice cover between 1972 and 2007 (National Ice Center, 2006). Retracted sea-ice creates open water areas where evaporation can occur from the Chukchi and Beaufort Seas in late summer and early autumn.

$\delta^{18}O_{wc}$ are not solely due to the strong covariance of sea-ice and air temperature. Evidence for this comes from the fact that summer sea-ice extent is negatively and significantly correlated with the residuals of the linear model regressing mean June temperature and $\delta^{18}O_{wc}$ in individual rings ($R = -0.26$). In summary, changes in both June temperature and sea-ice extent push $\delta^{18}O_{precip}$ values in the same direction. Therefore paleo-$\delta^{18}O_{wc}$ values provide a sensitive proxy record of prehistoric fluctuations in temperature change being amplified by the sea-ice albedo feedback.

5.2. Climatic controls over $\delta^{18}O_{wc}$ during the Younger Dryas

The most striking climatic change on the North Slope during the Pleistocene-Holocene transition occurred during the Younger Dryas (Figs. 7 and 8a). The shift to lower $\delta^{18}O_{wc}$ values during this time indicates significant summer-time cooling during the Younger Dryas in Arctic Alaska, which is consistent with other biological and geomorphic evidence from the region, including incision of floodplains, a standstill of paludification, the range retraction of extralimital cottonwood trees (Fig. 8b; Mann et al., 2010), sand dune reactivation (Gaglioti et al., in review), falling lake levels at LOP (Mann et al., 2002; Gaglioti et al., 2014), and a reduction in permafrost thaw (Fig. 8c; Gaglioti et al., 2014). Epstein (1995) also observed a comparable hydrogen isotope shift in subfossil willow cellulose during the Younger Dryas on the North Slope of Alaska (magnitude of isotopic change is converted to $\delta^{18}O_{wc}$ in Fig. 7). Significant Younger Dryas cooling on the North Slope of Alaska in winter has also been previously inferred from water-isotope values in an ice wedge near Barrow (Meyer et al., 2010).

To what degree were isotopic shifts during the Younger Dryas on the North Slope of Alaska influenced by local changes in temperature versus shifts in the geography of regional moisture sources that in turn were controlled by the seasonal extent of sea ice? The climatic excursion occurring during the Younger Dryas provides an interesting natural experiment into the sensitivity and utility of the $\delta^{18}O_{wc}$ for inferring changes in sea-ice cover and its amplifying effects. The magnitude of changes in smoothed $\delta^{18}O_{wc}$ values during the Younger Dryas amounted to a gradual lowering of ~4.5‰ that started ca. 13.0 ka, followed by a rapid rise of 4‰ between 11.8 and 11.2 ka (Fig. 7). During the Younger Dryas, rising sea level was probably just beginning to flood the Bering Strait (Keigwin et al., 2006; England and Furze, 2008; Hu et al., 2010; Jakobsson et al., 2017), so the major sources of precipitation for the North Slope at that time were either the North Pacific or the Arctic Ocean. Below

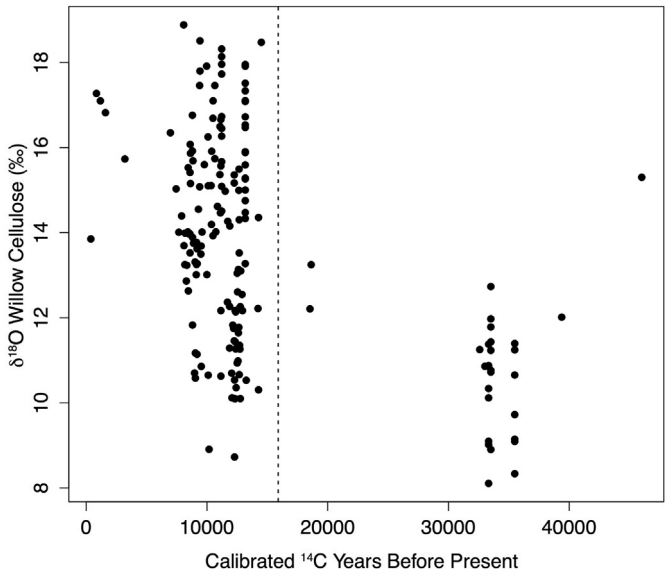

Fig. 6. Paleo-$\delta^{18}O_{wc}$ data from the North Slope of Alaska. Note the depleted values during much of the last ice age (before ~16 ka; denoted by the dashed line).

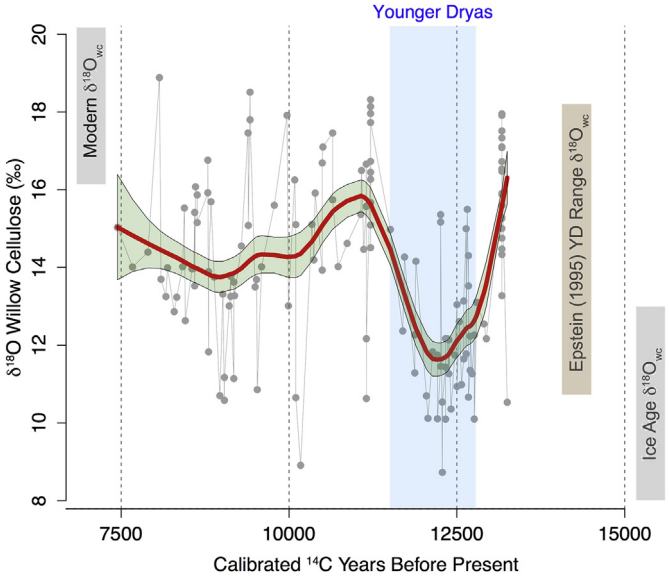

Fig. 7. Paleo-$\delta^{18}O_{wc}$ data for the Pleistocene-Holocene transition relative to $\delta^{18}O_{wc}$ from the last 30 years and during the last glacial period. The red line results from locally-weighted regression smoothing (LOWESS). The 95% confidence limit around this regression shown is in green. Blue shading is the Younger Dryas chronozone. Gray rectangles show the onestandard deviation range of $\delta^{18}O_{wc}$ values for modern samples (n = 263) shown to the left, and samples that date to 45.0–16.0 ka (n = 28), or the last ice age. Brown box shows the magnitude of Younger Dryas precipitation isotope change estimated for $\delta^{18}O_{wc}$ analyzed by Epstein (1995).

we consider two, alternative scenarios to explain the $\delta^{18}O_{wc}$ changes at the end of the Younger Dryas. In the first scenario, Younger Dryas temperatures cool on the North Slope during a time when the North Pacific is the main evaporative water source because the Arctic Ocean remains under perennial sea ice. The second scenario involves the North Slope cooling, but the evaporative source region for precipitation switches from the North Pacific to the Arctic Ocean under the assumption of declining sea ice

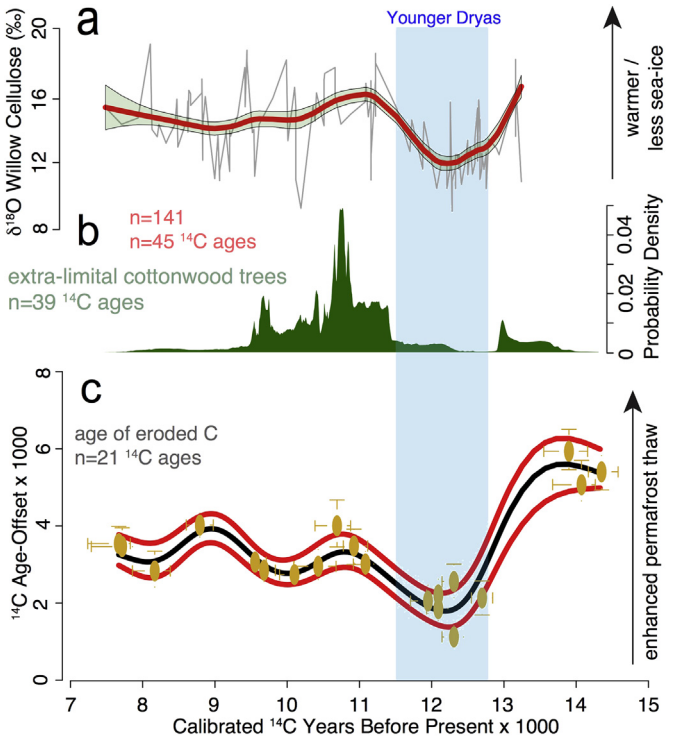

Fig. 8. Climate change and landscape responses on the North Slope of Alaska during the Younger Dryas. a) Willow isotope data from this study. Gray line is the raw data from individual pieces of wood. Red line is LOWESS smoothed data with a green 95% confidence interval. b) Cumulative probability density of 39 ^{14}C ages on the wood or leaves of cottonwood trees (*Populus balsamifera*) growing beyond current tree line. The presence of these extra-limital trees indicates a summer climate warmer than today (Mann et al., 2010). c) Radiocarbon age-offsets used as an index for the age of soil carbon eroding from watersheds. Yellow dots and bars show how much older the sediment coming into the lake was (y axis) at any given time between 15 and 7 ka (x axis). Black and red lines are interpolated mean and error of ^{14}C age offsets. Higher age offsets indicate enhanced permafrost thaw and the release of older carbon to lakes and streams. The Younger Dryas chronozone is shown in blue. The relatively warm Bølling-Allerød and the Holocene Thermal maximum occur immediately before and after the Younger Dryas.

responding to warming temperatures.

5.2.1. *Younger Dryas scenario 1: temperatures cool on the North Slope, but the North Pacific remains the primary moisture source*

The relatively large excursions in $\delta^{18}O_{wc}$ values observed during the Younger Dryas can only occur under a constant precipitation source if the North Pacific remained a relatively constant temperature, or in antiphase with local, North Slope temperature during the Pleistocene-Holocene transition. This is because that when local temperature ($T_{condensation}$ or T_c) and moisture source temperature (T_{source}) change in the same direction and with similar magnitudes, the net result is a relatively minor $\delta^{18}O_{precip}$ change (Fig. 9a; Epstein, 1995).

Based on paleoenvironmental records of sea surface temperatures in the North Pacific and air temperatures on the North Slope, we know that both places cooled and warmed in tandem during the Younger Dryas oscillation. Changes in ocean and atmospheric circulation resulted in a ~4 °C cooling in the North Pacific (T_{source}) during the Younger Dryas (Peteet and Mann, 1994; Max et al., 2012; Praetorius and Mix, 2014; Praetorius et al., 2015). A comparable ~4 °C cooling of growing season temperature on the North Slope (T_c) during the Younger Dryas is indicated by a southern retreat of tree-line and reduced permafrost thaw (Mann et al., 2002; Gaglioti et al., 2014). Estimating the $\delta^{18}O_{precip}$ using Rayleigh distillation

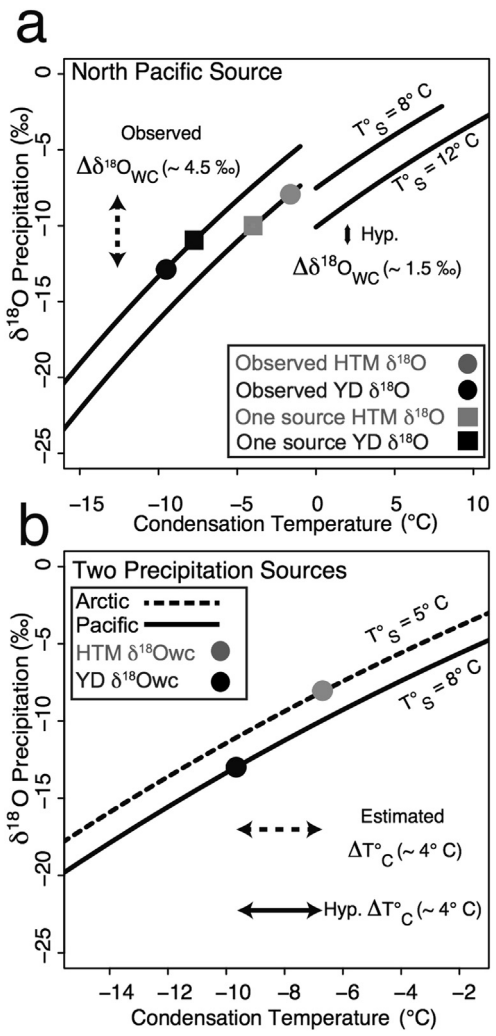

Fig. 9. a) Rayleigh distillation curve for precipitation coming from an 8 °C Pacific Ocean (T_{source} = 8 °C) during the Younger Dryas and a 12 °C Pacific Ocean (T_{source} = 12 °C) during the early Holocene (Praetorius et al., 2015). These curves illustrate how water vapor in an air mass becomes increasingly depleted in ^{18}O as it cools and loses water through condensation. Because changing T_{source} alters the starting point for the Rayleigh curves, a parallel change in T_c and T_{source} tends to produce minimal isotopic change for precipitation, if we assume the North Slope warmed by around 4 °C at the end of the Younger Dryas (Hypothesized change = 1.5‰; square points). The estimated isotopes in precipitation values (based on our $\delta^{18}O_{wc}$ data) during the Younger Dryas (black circle) and early Holocene (gray circle) show that the isotopic changes we observe cannot be explained by similar shifts in T_{source} and T_c because it would represent an unrealistic amount of T_c change (~8 °C warming) during the Younger Dryas to early Holocene transition. b) Rayleigh curves for precipitation sources coming from a cold ocean during the Holocene Thermal Maximum (HTM) (Arctic Ocean, T_{source} = 5 °C) and a warmer ocean during the YD (Pacific Ocean, T_{source} = 8 °C). This change of T_{source}, driven by sea-ice changes responding to climate, yields a reasonable estimate for T_c change that agrees with the paleobotanical evidence (a local T_c change in ~4 °C). Gray and black dots mark the hypothetical change of T_c and estimate $\delta^{18}O_{precip}$ on the North Slope from the Younger Dryas and HTM, respectively. These $\delta^{18}O_{precip}$ values are based on $\delta^{18}O_{wc}$.

modeling suggests that a 4 °C Younger Dryas cooling over the North Pacific *and* on the North Slope would result in only a ~1‰ change in $\delta^{18}O_{precip/wc}$ on the North Slope (Fig. 9a). Thus if moisture came solely from the North Pacific, changes in $\delta^{18}O_{precip/wc}$ would have been much less than actually observed during the Younger Dryas (~4–4.5‰) (Fig. 9a). If the precipitation source remained constant, a 4–4.5‰ change implies a T_c change of ~8 °C, which is an unreasonably large change in temperature based on the paleoenvironmental data. The North Slope $\delta^{18}O_{wc}$ record makes it highly unlikely that the North Pacific remained the sole moisture source for the North Slope throughout the Pleistocene-Holocene transition.

5.2.2. Scenario 2: changing moisture sources during the Younger Dryas

Our reconstructed $\delta^{18}O_{wc}$ record is most consistent with a shift between two different moisture sources that would cause T_c to be negatively correlated with T_{source} during the Younger Dryas climate oscillation. The 4–4.5‰ shift at the end of the Younger Dryas that we observe would agree with a 4 °C of warming on the North Slope only when the T_{source} change would involve a switch to a colder ocean (i.e., the Arctic Ocean or northern Bering Sea) during warm times (higher $\delta^{18}O_{wc}$) and to a warmer ocean (i.e., the North Pacific) during cold times (lower $\delta^{18}O_{wc}$) (Fig. 9b). These antiphase shifts in $T_{source} - T_c$ were possible because the Arctic Ocean is always colder than the North Pacific even when it would become the T_{source} during warm times.

In summary, although it would have contributed to isotopic changes, the combination of local temperature change (T_c) and a constant precipitation source from the ice-free North Pacific can only explain ~25% of the $\delta^{18}O_{wc}$ changes we observe during the Younger Dryas on Alaska's North Slope. Instead, the paleo-$\delta^{18}O_{wc}$ fluctuations we see are most likely the outcome of a combination of local temperature changes *plus* changes in precipitation sources between the Arctic Ocean (during warm periods) and the North Pacific (during cool periods).

As it does today on an inter- and intra-annual scale, sea ice probably played a role in controlling the location of the dominant moisture sources for Arctic precipitation during the Pleistocene–Holocene transition. During the Allerød warm period preceding the Younger Dryas, reduced summer sea-ice cover would have allowed more evaporation from the relatively cold waters of the Arctic Ocean and northern Bering Sea, with the result that $\delta^{18}O_{wc}$ values were higher than they would be if only local warming was affecting them (Fig. 10). Because sea level was reduced by ~70 m during this time (Lambeck et al., 2014), and much of the Northern Bering and Chukchi Sea was exposed land masses to the northwest of our study site (Fig. 10), air masses going over the relatively ice-free Beaufort Sea to the northeast would have carried these local moisture sources. A northeasterly-dominated wind pattern is also supported by the orientation of longitudinal dunes that were active during the full glacial and Lateglacial periods (Carter, 1981). In contrast, during the Younger Dryas, cooler temperatures coupled with a massive freshwater outburst flood from the Mackenzie River (Murton et al., 2010; Condron and Winsor, 2012) would have enhanced sea-ice coverage (Bradley and England, 2008; Condron and Winsor, 2012; Not and Hillaire-Marcel, 2012), capping these cold water sources and relegating moisture sources to the warmer North Pacific. In response, $\delta^{18}O_{wc}$ values during the Younger Dryas were lower than they would have been if it was only local cooling was affecting them (Fig. 10). This sea ice modulation of precipitation could also explain why glacier advances in the Brooks Range dating to the Younger Dryas appear to be absent (Briner and Kaufman, 2008; Badding et al., 2013; Pendleton et al., 2015; but also see Hamilton, 1982) because increased sea ice during this cold time would have starved glaciers of precipitation.

Sea-ice controlled switching between different oceanic evaporative sources is seen in other Arctic regions during Late Glacial times. Sea-ice modulation of precipitation is invoked to explain greater $\delta^{18}O_{precip}$ and D excess values during warm times in the Greenland ice cores (Jouzel et al., 2005). Such a scenario is also supported by paleo-records of sea-ice coverage from the Chukchi and Beaufort Seas, as well as modeling results, that indicate enhanced sea-ice cover during the Younger Dryas followed by

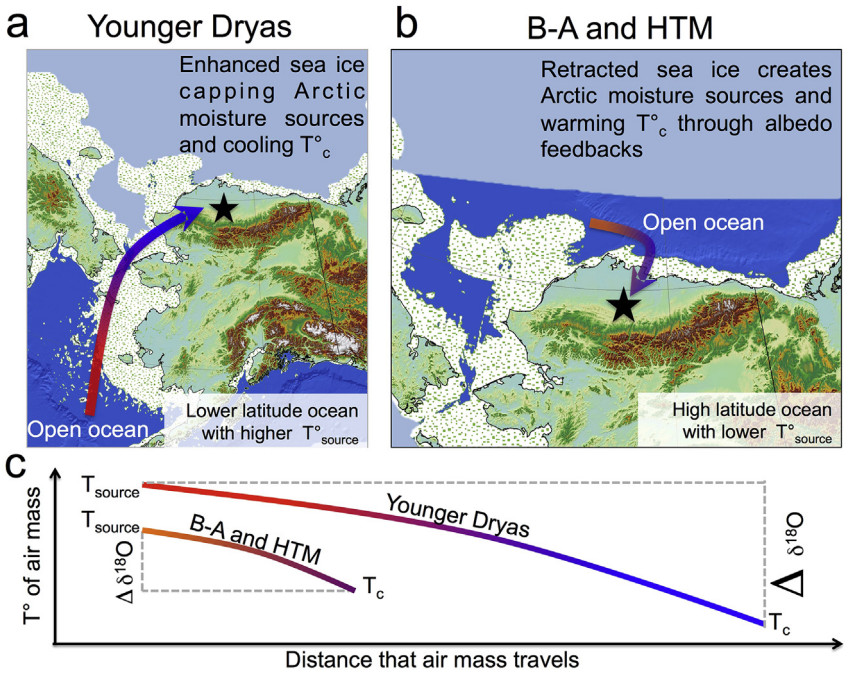

Fig. 10. Conceptual model showing how changes in sea ice during the Pleistocene-Holocene transition affected temperature and $\delta^{18}O_{wc}$ on the North Slope of Alaska. Maps showing the geography of Alaska and Siberia at ~12 ka when sea level was lowered by 50 m (off-white with green shading; from Amante and Eakins, 2009), and today (topo maps with black outline). a) Enhanced perennial sea ice (light blue area) during the Younger Dryas cold interval, which further cools local temperatures on the North Slope due to albedo feedbacks (low T_c or low local temperatures on the North Slope) and relegate its moisture sources to the Southern Bering and North Pacific, which have relatively high T_{source}. b) Directly before and after the Younger Dryas during the warm Bølling Allerød (B-A), and Holocene Thermal Maximum (HTM), sea-ice extent would have been reduced, which contributed to local warming through albedo feedbacks (high T_c). The seasonally ice-free Chukchi and Beaufort Seas would have become evaporative moisture sources for precipitation (low T_{source}) during these relatively warm times. c) Because of the antiphase relationship between T_{source} and T_c during these climate oscillations, this scenario creates large shifts in water isotope changes recorded by subfossil willows on the North Slope. During the Younger Dryas, a relatively high T_{source} that is far away coupled with a low T_c enhances the isotopic depletion of ^{18}O in precipitation fueling willow growth (large Δ). During the B-A and HTM warm times, a lower T_{source} that is adjacent to the North Slope, coupled with a higher T_c, reduces the amount of isotopic depletion of ^{18}O in precipitation (small Δ). Changes in sea ice extent responding to these climate oscillations enhances local climate and isotopic change in the Arctic regions of Alaska.

reduced ice cover during the early Holocene (Cook et al., 2005; Caissie et al., 2010; Polyak et al., 2010; Condron and Winsor, 2012; Not and Hillaire-Marcel, 2012; Riethdorf et al., 2013). Just as they do today, these sea-ice responses would have amplified the local expression of global climate events such as those caused by a shutdown of the thermohaline circulation during the Younger Dryas and orbitally-driven warming and cooling during the early and late Holocene (i.e. Holocene Thermal Maximum and the Neoglacial period).

5.3. Was there an isotopic signature of the Bering Land Bridge flooding?

The gradual $\delta^{18}O_{wc}$ decrease of ~1.5‰ occurring between 11.0 and 10.0 ka (Fig. 7) is also seen in Epstein's (1995) δD record based on subfossil willow cellulose from the North Slope. We suspect this cooling event represents the advent of more maritime climatic conditions as relative sea level (RSL) rose and the coastlines of the Arctic Ocean and Bering Sea approached our study sites. Between 11.5 and 9.5 ka, rising RSL flooded around 65% of the now-submerged continental shelf adjacent to North Slope that had been exposed during the last glacial maximum (Mann et al., 2001). Cooler growing season temperatures, increases in precipitation, and decreases in intra-annual temperature variability would have accompanied the rapidly approaching shoreline (Mock et al., 1998; Mann et al., 2001). In addition, the flooding of the Bering Strait and the influx of warm and relatively fresh (lower $\delta^{18}O_{precip}$ values) Pacific water may have further reduced $\delta^{18}O_{precip/wc}$ on the North Slope due to lower $\delta^{18}O$ values of the evaporative moisture source and warming T_{source} effects on precipitation (illustrated in Figs. 9 and 10).

Although the timing of the initial flooding of Bering Shelf has been investigated for decades, it is still uncertain when significant ocean currents first entered the Arctic Ocean from the North Pacific and significantly warmed/freshened the Chukchi Sea (Overland and Roach, 1987; Keigwin et al., 2006; England and Furze, 2008; Hu et al., 2010), but the likely age estimate is ~11.0 ka (Jakobsson et al., 2017). We hypothesize that the 11.0–10.0 ka lowering of $\delta^{18}O_{wc}$ may record these oceanic events and their effects on ocean currents, $\delta^{18}O_{precip}$, and North Slope air temperatures.

5.4. How the present climate compares to the past

The $\delta^{18}O$ data indicate the North Slope is now experiencing climatic conditions slightly warmer than the previously warmest times of the last 13.5 ka. Today, willow $\delta^{18}O_{wc}$ values have a mean of 18.03‰, which is more than 2.5‰ (the combined uncertainty due to site and stem variability) higher than the highest smoothed values dating from the early Holocene warm period and from just before the Younger Dryas during the Bølling-Allerød interstadial (Fig. 7). This is both interesting and alarming because both of these prehistoric warm times saw widespread thermokarsting, rapid floodplain aggradation (Mann et al., 2010), and sweeping changes in both the flora and the fauna of northern Alaska (Fig. 8; Mann et al., 2002, Mann et al., 2013). A resumption of these temperature-related effects will have similarly large-scale biophysical responses and feedbacks.

6. Conclusions

Using a time series of $\delta^{18}O$ values in ^{14}C-dated wood, we describe a multi-millennial record of climate change on the North Slope of Alaska. The $\delta^{18}O_{wc}$ values of willows now growing at upland tundra sites are positively correlated with air temperatures and negatively correlated with both distance from the Chukchi Sea and Beaufort Sea and with the extent of Arctic sea ice in summer. Sea-ice cover exerts its effects on $\delta^{18}O$ values in willow cellulose in two, mutually reinforcing ways. First, the sea-ice-albedo effect modulates air temperatures over the North Slope by making summers warmer when sea-ice is less extensive and vice versa. Second, the areal extent of sea ice influences the geographic distribution of evaporative source areas in Arctic seas that supply precipitation isotopes with relatively high $\delta^{18}O$ values to the North Slope willows. This means that air temperature and sea-ice extent act in synergy to drive $\delta^{18}O_{wc}$ in the same direction.

Based on these modern, isotope-climate-geography relationships, we used a time series of $\delta^{18}O_{wc}$ values from analyses of ancient wood to make inferences about past climates and the processes responsible for creating them. Prior to ca. ~16 ka, climate on the North Slope was highly continental, with $\delta^{18}O_{wc}$ values lower than those dating to post-glacial times. Air temperatures were lower and evaporative source areas for moisture were more distant and further south. Younger Dryas cooling is recorded in the $\delta^{18}O_{wc}$ record from the North Slope with a ~4–4.5‰ shift to lower $\delta^{18}O_{wc}$ values between 12.9 and 11.7 ka. This and other deglacial climate events known from the North Atlantic were possibly amplified on the North Slope through the effects of the sea ice-albedo feedback on air temperatures and moisture sources. Today's $\delta^{18}O_{wc}$ values on the North Slope are now elevated compared with those dating to the warmest part of post-glacial times (~13.2, 11.3–9.0 ka), which was accompanied by widespread permafrost degradation and rapid changes in the geographic ranges of the biota.

Acknowledgements

The National Institute of Water Resources Alaska division funded this study along with the National Science Foundation (NSF grants: PLR-1417036 and 1417611) and the Bureau of Land Management. We thank Dan Cross-Call, Andrew Weller, Joe Gaglioti, and Louise Farquharson for help in the field. Nick Wiesenburg helped with cross-dating shrub rings. Kim Sparks, Shane Billings, Tim Howe, and Norma Haubenstock contributed greatly to cellulose extractions. We benefitted from discussions with Eric Klein, Jeff Welker, Bruce Finney, Laia Andreu-Hayles, and Lesleigh Anderson. Comments from Trevor Porter and an anonymous reviewer improved this manuscript. Any use of trade, product, or firm names is for descriptive purposes only and does not imply endorsement by the U.S. Government. This is LDEO contribution #8113.

Appendix A. Supplementary data

Supplementary data related to this article can be found at http://dx.doi.org/10.1016/j.quascirev.2017.05.012.

References

Ager, T.A., Axford, Y., Balascio, N.L., Begét, J.E., Brigham-Grette, J., Briner, J.P., Bundtzen, T.K., Carrara, P., Hamilton, T.D., Lubinski, D.J., 2004. Pleistocene maximum and Late Wisconsinan glacier extents across Alaska, USA. Quat. Glaciations-Extent Chronology Part II N. Am. 2, 9.

Alexeev, V.A., Arp, C.D., Jones, B.M., Cai, L., 2016. Arctic sea ice decline contributes to thinning lake ice trend in northern Alaska. Environ. Res. Lett. 11, 74022.

Alley, R.B., 2000. The Younger Dryas cold interval as viewed from central Greenland. Quat. Sci. Rev. 19, 213–226.

Amante, C., Eakins, B.W., 2009. ETOPO1 1 Arc-minute Global Relief Model: Procedures, Data Sources and Analysis. NOAA Technical Memorandum NESDIS NGDC-24. National Geophysical Data Center, NOAA. http://dx.doi.org/10.7289/V5C8276M.

Badding, M.E., Briner, J.P., Kaufman, D.S., 2013. ^{10}Be ages of late pleistocene deglaciation and Neoglaciation in the North-central Brooks range, arctic Alaska. J. Quat. Sci. 28, 95–102.

Baughman, C.A., Mann, D.H., Verbyla, D.L., Kunz, M.L., 2015. Soil-surface organic layers in Arctic Alaska: spatial distribution, rates of formation, microclimatic effects. J. Geophys. Res. Biogeosciences 120, 1150–1164.

Bhatt, U.S., Walker, D.A., Walsh, J.E., Carmack, E.C., Frey, K.E., Meier, W.N., Moore, S.E., Parmentier, F.J.W., Post, E., Romanovsky, V.E., Simpson, W.R., 2014. Implications of arctic sea ice decline for the earth system. Annu. Rev. Environ. Resour. 39, 57–89.

Bintanja, R., van de Wal, R.S., Oerlemans, J., 2005. Modelled atmospheric temperatures and global sea levels over the past million years. Nature 437, 125–128.

Boisvert, L.N., Stroeve, J.C., 2015. The Arctic is becoming warmer and wetter as revealed by the Atmospheric Infrared Sounder. Geophys. Res. Lett. 42, 4439–4446.

Bowen, G.J., Wilkinson, B., 2002. Spatial distribution of $\delta^{18}O$ in meteoric precipitation. Geology 30, 315–318.

Bradley, R.S., England, J.H., 2008. The younger Dryas and the sea of ancient ice. Quat. Res. 70, 1–10.

Brienen, R.J.W., Helle, G., Pons, T.L., Guyot, J.L., Gloor, M., 2012. Oxygen isotopes in tree rings are a good proxy for Amazon precipitation and El Niño-Southern Oscillation variability. Proc. Natl. Acad. Sci. 109, 16957–16962.

Briner, J.P., Kaufman, D.S., 2008. Late Pleistocene mountain glaciation in Alaska: key chronologies. J. Quat. Sci. 23, 659–670.

Burk, R.L., Stuiver, M., 1981. Oxygen isotope ratios in trees reflect mean annual temperature and humidity. Science 211, 1417–1419.

Caissie, B.E., Brigham-Grette, J., Lawrence, K.T., Herbert, T.D., Cook, M.S., 2010. Last Glacial Maximum to Holocene sea surface conditions at Umnak Plateau, Bering Sea, as inferred from diatom, alkenone, and stable isotope records. Paleoceanography 25, PA1206.

Carter, L.D., 1981. A pleistocene sand sea on the Alaskan arctic coastal plain. Science 211, 381–383.

Clark, I.D., Fritz, P., 1997. Environmental Isotopes in Hydrogeology. CRC Press, Boca Raton.

Cleveland, W.S., Devlin, S.J., 1988. Locally weighted regression: an approach to regression analysis by local fitting. J. Am. Stat. Assoc. 83, 596–610.

Cleveland, W.S., Loader, C., 1996. Smoothing by local regression: principles and methods. In: Statistical Theory and Computational Aspects of Smoothing. Physica-Verlag HD, pp. 10–49.

Condron, A., Winsor, P., 2012. Meltwater routing and the younger Dryas. Proc. Natl. Acad. Sci. 109, 19928–19933.

Cook, M.S., Keigwin, L.D., Sancetta, C.A., 2005. The deglacial history of surface and intermediate water of the Bering Sea. Deep Sea Res. Part II Top. Stud. Oceanogr. 52, 2163–2173.

Deser, C., Tomas, R., Alexander, M., Lawrence, D., 2010. The seasonal atmospheric response to projected Arctic sea ice loss in the late twenty-first century. J. Clim. 23, 333–351.

England, J.H., Furze, M.F.A., 2008. New evidence from the western canadian arctic archipelago for the resubmergence of Bering Strait. Quat. Res. 70, 60–67.

Epstein, S., 1995. The isotopic climatic records in the Allerød-Bølling-Younger Dryas and Post-Younger Dryas events. Glob. Biogeochem. Cycles 9, 557–563.

Epstein, S., Yapp, C.J., Hall, J.H., 1976. The determination of the D/H ratio of non-exchangeable hydrogen in cellulose extracted from aquatic and land plants. Earth Planet. Sci. Lett. 30, 241–251.

Fetterer, F., Knowles, K., Meier, W., Savoie, M., 2002. Sea Ice Index, Version 1. NSIDC: National Snow and Ice Data Center, Boulder, Colorado USA. http://dx.doi.org/10.7265/N5QJ7F7W.

Gaglioti, B.V., Mann, D.H., Jones, B.M., Pohlman, J.W., Kunz, M.L., Wooller, M.J., 2014. Radiocarbon age-offsets in an arctic lake reveal the long-term response of permafrost carbon to climate change. J. Geophys. Res. Biogeosciences 119, 1630–1651.

Gaglioti, B.V., Mann, D.H., Groves, P., Kunz, M.L., Wooller, M.J., Farquharson, L.M., Jones, B.J., Reanier, R.E., (In Review). Sedimentary sequences from unglaciated Arctic Alaska describe climate forcing and landscape responses during the last ice age. Quaternary Science Reviews.

Goff, J.A., Gratch, S., 1946. Low-pressure properties of water from -160° to 212° F. Trans. Am. Soc. Heat. Vent. Eng. 51, 125–164.

Gray, J., Thompson, P., 1977. Climatic information from $^{18}O/^{16}O$ analysis of cellulose, lignin and whole wood from tree rings. Nature 270 (5639), 708–709.

Green, J.W., 1963. Wood cellulose. In: Methods in Carbohydrate Chemistry, Vol. 3: Cellulose. Academic Press, pp. 9–20.

Hamilton, T.D., 1982. A Late Pleistocene glacial chronology for the southern Brooks Range: stratigraphic record and regional significance. Geol. Soc. Am. Bull. 93, 700–716.

Harris, I., Jones, P.D., Osborn, T.J., Lister, D.H., 2014. Updated high-resolution grids of monthly climatic observations–the CRU TS3. 10 Dataset. Int. J. Climatol. 34, 623–642.

Hinkel, K.M., Nelson, F.E., 2003. Spatial and temporal patterns of active layer thickness at Circumpolar Active Layer Monitoring (CALM) sites in northern

Alaska, 1995–2000. J. Geophys. Res. Atmos. 108 (8168), D2.
Holmes, R.L., 1983. Computer-assisted quality control in tree-ring dating and measurement. Tree-ring Bull. 43, 69–78.
Homan, J., 2015. Precipitation in the Alaska Central Arctic. University of Alaska Fairbanks Dissertation.
Hu, A., Meehl, G.A., Otto-Bliesner, B.L., Waelbroeck, C., Han, W., Loutre, M.F., Lambeck, K., Mitrovica, J.X., Rosenbloom, N., 2010. Influence of Bering Strait flow and North Atlantic circulation on glacial sea-level changes. Nat. Geosci. 3, 118–121.
Jakobsson, M., Andreassen, K., Bjarnadóttir, L.R., Dove, D., Dowdeswell, J.A., England, J.H., Funder, S., Hogan, K., Ingólfsson, Ó., Jennings, A., Larsen, N.K., 2014. Arctic Ocean glacial history. Quat. Sci. Rev. 92, 40–67.
Jakobsson, et al., 2017. Post-glacial flooding of the Beringia land bridge dated to 11,000 cal yrs BP based on new geophysical and sediment records. Clim. Past Discuss. http://dx.doi.org/10.5194/cp-2017-11, 2017.
Jeffries, M.O., Richter-Menge, J.A., Overland, J.E., 2012. Arctic Report Card 2012. http://www.arctic.noaa.gov/reportcard.
Jorgenson, M.T., Shur, Y.L., Pullman, E.R., 2006. Abrupt increase in permafrost degradation in Arctic Alaska. Geophys. Res. Lett. 33, L02503.
Jorgenson, M.T., Yoshikawa, K., Kanevskiy, M., Shur, Y., Romanovsky, V., Marchenko, S., Grosse, G., Brown, J., Jones, B., 2008. Permafrost Characteristics of Alaska. Institute of Northern Engineering, University of Alaska, Fairbanks.
Jouzel, J., Masson-Delmotte, V., Stiévenard, M., Landais, A., Vimeux, F., Johnsen, S.J., Sveinbjörnsdottir, A.E., White, J.W., 2005. Rapid deuterium-excess changes in Greenland ice cores: a link between the ocean and the atmosphere. Comptes Rendus Geosci. 337, 957–969.
Kaufman, D.S., Ager, T.A., Anderson, N.J., Anderson, P.M., Andrews, J.T., Bartlein, P.J., Brubaker, L.B., Coats, L.L., Cwynar, L.C., Duvall, M.L., Dyke, A.S., et al., 2004. Holocene thermal maximum in the western Arctic (0-180°W). Quat. Sci. Rev. 23, 529–560.
Kaufman, D.S., Axford, Y.L., Henderson, A.C., McKay, N.P., Oswald, W.W., Saenger, C., Anderson, R.S., Bailey, H.L., Clegg, B., Gajewski, K., Hu, F.S., 2016. Holocene climate changes in eastern Beringia (NW North America)–A systematic review of multi-proxy evidence. Quat. Sci. Rev. 147, 312–339.
Keigwin, L.D., Donnelly, J.P., Cook, M.S., Driscoll, N.W., Brigham-Grette, J., 2006. Rapid sea-level rise and Holocene climate in the Chukchi sea. Geology 34, 861–864.
Kendall, C., McDonnell, J.J., 2012. Isotope Tracers in Catchment Hydrology. Elsevier.
Klein, E.S., Cherry, J.E., Young, J., Noone, D., Leffler, A.J., Welker, J.M., 2015a. Arctic cyclone water vapor isotopes support past sea ice retreat recorded in Greenland ice. Sci. Rep. 5, 10295.
Klein, E.S., Nolan, M., McConnell, J., Sigl, M., Cherry, J., Young, J., Welker, J.M., 2015b. McCall Glacier record of Arctic climate change: interpreting a northern Alaska ice core with regional water isotopes. Quat. Sci. Rev. 131, 274–284.
Kopec, B.G., Feng, X., Michel, F.A., Posmentier, E.S., 2016. Influence of sea ice on Arctic precipitation. Proc. Natl. Acad. Sci. 113, 46–51.
Lambeck, K., Rouby, H., Purcell, A., Sun, Y., Sambridge, M., 2014. Sea level and global ice volumes from the last glacial maximum to the Holocene. Proc. Natl. Acad. Sci. 111, 15296–15303.
Lambers, H., Pons, T.L., Chapin III, F.S., 1998. Plant Physiological Ecology.
Leavitt, S.W., 2010. Tree-ring C–H–O isotope variability and sampling. Sci. Total Environ. 408, 5244–5253.
Leavitt, S.W., Danzer, S.R., 1993. Method for batch processing small wood samples to holocellulose for stable-carbon isotope analysis. Anal. Chem. 65, 87–89.
Majoube, M., 1970. Fractionation factor of 18O between water vapour and ice. Nature 242, 1242.
Majoube, M., 1971. Oxygen-18 and deuterium fractionation between water and steam. J. de Chimie Physique de Physico-Chimie Biol. 68, 1423.
Mann, D.H., Reanier, R.E., Peteet, D.M., Kunz, M.L., Johnson, M., 2001. Environmental change and Arctic paleoindians. Arct. Anthropol. 38 (2), 119–138.
Mann, D.H., Peteet, D.M., Reanier, R.E., Kunz, M.L., 2002. Responses of an arctic landscape to Lateglacial and early Holocene climatic changes: the importance of moisture. Quat. Sci. Rev. 21, 997–1021.
Mann, D.H., Groves, P., Reanier, R.E., Kunz, M.L., 2010. Floodplains, permafrost, cottonwood trees, and peat: what happened the last time climate warmed suddenly in Arctic Alaska? Quat. Sci. Rev. 29, 3812–3830.
Mann, D.H., Groves, P., Kunz, M.L., Reanier, R.E., Gaglioti, B.V., 2013. Ice-age megafauna in Arctic Alaska: extinction, invasion, survival. Quaternary Sci. Rev. 70, 91–108.
Max, L., Riethdorf, J.R., Tiedemann, R., Smirnova, M., Lembke Jene, L., Fahl, K., Nürnberg, D., Matul, A., Mollenhauer, G., 2012. Sea surface temperature variability and sea-ice extent in the subarctic northwest Pacific during the past 15,000 years. Paleoceanography 27, PA3213.
McCarroll, D., Loader, N.J., 2004. Stable isotopes in tree rings. Quat. Sci. Rev. 23, 771–801.
Melles, M., Brigham-Grette, J., Minyuk, P.S., Nowaczyk, N.R., Wennrich, V., DeConto, R.M., Anderson, P.M., Andreev, A.A., Coletti, A., Cook, T.L., Haltia-Hovi, E., Kukkonen, M., Lozhkin, A.V., Rosen, P., Tarasov, P., Vogel, H., Wagner, B., 2012. 2.8 million years of arctic climate change from lake El'gygytgyn, NE Russia. Science 337, 315–320.
Meyer, H., Schirrmeister, L., Yoshikawa, K., Opel, T., Wetterich, S., Hubberten, H.W., Brown, J., 2010. Permafrost evidence for severe winter cooling during the Younger Dryas in northern Alaska. Geophys. Res. Lett. 37, L03501.
Mock, C.J., Bartlein, P.J., Anderson, P.M., 1998. Atmospheric circulation patterns and spatial climatic variations in Beringia. Int. J. Climatol. 18 (10), 1085–1104.
Moritz, R.E., 1979. Synoptic Climatology of the Beaufort Sea Coast of Alaska. Institute of Arctic and Alpine Research, Boulder, CO.
Murton, J.B., Bateman, M.D., Dallimore, S.R., Teller, J.T., Yang, Z., 2010. Identification of younger Dryas outburst flood path from lake agassiz to the Arctic Ocean. Nature 464, 740–743.
National Ice Center, 2006. updated 2009. In: Fetterer, F., Fowler, C. (Eds.), National Ice Center Arctic Sea Ice Charts and Climatologies in Gridded Format. National Snow and Ice Data Center, Boulder, Colorado USA. http://dx.doi.org/10.7265/N5X34VDB.
Not, C., Hillaire-Marcel, C., 2012. Enhanced sea-ice export from the arctic during the younger Dryas. Nat. Commun. 3, 647.
Overland, J.E., Roach, A.T., 1987. Northward flow in the Bering and Chukchi seas (1984–2012). J. Geophys. Res. Atmos. 92, 7097–7105.
Pendleton, S.L., Ceperley, E.G., Briner, J.P., Kaufman, D.S., Zimmerman, S., 2015. Rapid and early deglaciation in the central Brooks range, Arctic Alaska. Geology 43, 419–422.
Peteet, D.M., Mann, D.H., 1994. Late-glacial vegetational, tephra, and climatic history of southwestern Kodiak Island, Alaska. Ecoscience 1, 255–267.
Polyak, L., Alley, R.B., Andrews, J.T., Brigham-Grette, J., Cronin, T.M., Darby, D.A., Dyke, A.S., Fitzpatrick, J.J., Funder, S., Holland, M., 2010. History of sea ice in the Arctic. Quat. Sci. Rev. 29, 1757–1778.
Porter, T.J., Pisaric, M.F., Kokelj, S.V., Edwards, T.W., 2009. Climatic signals in $\delta^{13}C$ and $\delta^{18}O$ of tree-rings from white spruce in the Mackenzie Delta region, northern Canada. Arct. Antarct. Alp. Res. 41, 497–505.
Porter, T.J., Middlestead, P., 2012. On estimating the precision of stable isotope ratios in processed tree-rings. Dendrochronologia 30, 239–242.
Post, E., Forchhammer, M.C., Bret-Harte, M.S., Callaghan, T.V., Christensen, T.R., Elberling, B., Fox, A.D., Gilg, O., Hik, D.S., Høye, T.T., Ims, R.A., 2009. Ecological dynamics across the Arctic associated with recent climate change. Science 325, 1355–1358.
Praetorius, S.K., Mix, A.C., 2014. Synchronization of North Pacific and Greenland climates preceded abrupt deglacial warming. Science 345, 444–448.
Praetorius, S.K., Mix, A.C., Walczak, M.H., Wolhowe, M.D., Addison, J.A., Prahl, F.G., 2015. North Pacific deglacial hypoxic events linked to abrupt ocean warming. Nature 527, 362–366.
Putman, A.L., 2013. Tracking the Moisture Sources of Storms at Barrow, Alaska: Seasonal Variations and Isotopic Characteristics. Masters Thesis. Dartmouth College.
Reimer, P.J., Bard, E., Bayliss, A., Beck, J.W., Blackwell, P.G., Bronk Ramsey, C., Buck, C.E., Cheng, H., Edwards, R.L., Friedrich, M., 2013. IntCal13 and Marine13 radiocarbon age calibration curves 0-50,000 years cal BP. Radiocarbon 55, 1869–1887.
Richter, S.L., Johnson, A.H., Dranoff, M.M., LePage, B.A., Williams, C.J., 2008. Oxygen isotope ratios in fossil wood cellulose: isotopic composition of Eocene-to Holocene-aged cellulose. Geochimica Cosmochimica Acta 72, 2744–2753.
Riethdorf, J.R., Max, L., Nürnberg, D., Lembke Jene, L., Tiedemann, R., 2013. Deglacial development of (sub) sea surface temperature and salinity in the subarctic northwest Pacific: implications for upper-ocean stratification. Paleoceanography 28, 91–104.
Roden, J.S., Lin, G., Ehleringer, J.R., 2000. A mechanistic model for interpretation of hydrogen and oxygen isotope ratios in tree-ring cellulose. Geochimica Cosmochimica Acta 64, 21–35.
Romanovsky, V.E., Osterkamp, T.E., 1995. Interannual variations of the thermal regime of the active layer and near-surface permafrost in northern Alaska. Permafr. Periglac. Process. 6, 313–335.
Ruddiman, W.F., 2001. Earth's Climate: Past and Future. Macmillan.
Schleser, G.H., Frielingsdorf, J., Blair, A., 1999. Carbon isotope behaviour in wood and cellulose during artificial aging. Chem. Geol. 158, 121–130.
Schuur, E.A.G., Bockheim, J., Canadell, J.G., Euskirchen, E., Field, C.B., Goryachkin, S.V., Hagemann, S., Kuhry, P., Lafleur, P.M., Lee, H., Mazhitova, G., Nelson, F.E., Rinke, A., Romanovsky, V.E., Shiklomanov, N., Tarnocai, C., Venevsky, S., Vogel, J.G., Zimov, S.A., 2008. Vulnerability of permafrost carbon to climate change: implications for the global carbon cycle. BioScience 58, 701.
Screen, J.A., Simmonds, I., 2010. The central role of diminishing sea ice in recent Arctic temperature amplification. Nature 464, 1334–1337.
Serreze, M.C., Francis, J.A., 2006. The Arctic amplification debate. Clim. Change 76, 241–264.
Sidorova, O.V., Siegwolf, R.T., Saurer, M., Naurzbaev, M.M., Shashkin, A.V., Vaganov, E.A., 2010. Spatial patterns of climatic changes in the Eurasian north reflected in Siberian larch tree-ring parameters and stable isotopes. Glob. Change Biol. 16, 1003–1018.
Smith, S.L., Romanovsky, V.E., Lewkowicz, A.G., Burn, C.R., Allard, M., Clow, G.D., Yoshikawa, K., Throop, J., 2010. Thermal state of permafrost in North America: a contribution to the international polar year. Permafr. Periglac. Process. 21 (2), 117–135.
Sternberg, L.D.S., Deniro, M.J., Savidge, R.A., 1986. Oxygen isotope exchange between metabolites and water during biochemical reactions leading to cellulose synthesis. Plant Physiol. 82, 423–427.
Szymczak, S., Joachimski, M.M., Bräuning, A., Hetzer, T., Kuhlemann, J., 2011. Comparison of whole wood and cellulose carbon and oxygen isotope series from *Pinus nigra* ssp. laricio (Corsica/France). Dendrochronologia 29, 219–226.
Vihma, T., 2014. Effects of Arctic sea ice decline on weather and climate: a review. Surv. Geophys. 35, 1175–1214.
Walker, D.A., Raynolds, M.K., Daniëls, F.J., Einarsson, E., Elvebakk, A., Gould, W.A., Katenin, A.E., Kholod, S.S., Markon, C.J., Melnikov, E.S., Moskalenko, N.G., 2005.

The circumpolar Arctic vegetation map. J. Veg. Sci. 16, 267–282.
Wendler, G., Shulski, M., Moore, B., 2010. Changes in the climate of the alaskan North Slope and the ice concentration of the adjacent Beaufort sea. Theor. Appl. Climatol. 99, 67–74.
Wendler, G., Moore, B., Galloway, K., 2014. Strong temperature increase and shrinking sea ice in Arctic Alaska. Open Atmos. Sci. J. 8, 7–15.
Yapp, C.J., Epstein, S., 1982. A reexamination of cellulose carbon-bound hydrogen δD measurements and some factors affecting plant-water D/H relationships. Geochimica Cosmochimica Acta 46, 955–965.
Zhang, T., Osterkamp, T.E., Stamnes, K., 1996. Some characteristics of the climate in northern Alaska. USA. Arct. Alp. Res. 28, 509–518.